

Electroreflectance Study of Gold Nanoparticles Immobilized on an Aminoalkanethiol Monolayer Coated on a Polycrystalline Gold Electrode Surface

Takamasa Sagara,^{*,†,‡} Naoyuki Kato,[‡] and Naotoshi Nakashima[‡]

“Organization and Function”, PRESTO, JST, Japan, and Department of Materials Science, Graduate School of Science and Technology, Nagasaki University, Bunkyo 1-14, Nagasaki 852-8521, Japan

Received: May 10, 2001; In Final Form: October 5, 2001

Citrate-stabilized gold (Au) nanoparticles of a diameter of 11 nm were immobilized on a monolayer of aminoundecanethiol (1-mercapto-11-aminoundecane) coated on a polycrystalline Au electrode surface. A quartz crystal microbalance measurement of the deposition process of the Au particles revealed that the saturated deposition amount is 10% of a 2D close-packed monolayer, and this coverage was confirmed by an atomic force microscopy (AFM) observation. The Au particle layer was characterized by the use of potential-modulated UV–visible reflectance spectroscopy (electroreflectance spectroscopy). The electroreflectance (ER) band at the plasmon absorption wavelength of the Au particles was positive-going, indicating that the plasmon absorption becomes stronger when changing the electrode potential to more negative. The plasmon absorption band shifted to longer wavelength when the electrode potential approaches to the potential of zero-charge, E_{pzc} , of the Au electrode. The ER signal intensity also showed a maximum around E_{pzc} . In light of good electronic communication between the Au electrode substrate and the deposited Au particles as demonstrated by reversible redox waves of solution phase species, the ER signal was interpreted as being originated from the potential-dependent charging–discharging process of the immobilized Au particles; a more negatively charged Au particle exhibits a stronger and sharper plasmon absorption band at a shorter wavelength. The implications of the ER signal were discussed.

Introduction

Modification of electrode surfaces with metal nanoparticles has recently been drawing attention from both theoretical and application viewpoints.^{1–12} Emergence of various specific properties of the metal nanoparticles at an electrode/solution interface is regarded as being among the novel strategies to functionalize electrode surfaces, leading to the construction of nanoscale devices. Gold (Au) nanoparticles can be immobilized as an organized mono- or multiparticle layer on a solid surface with the help of a long-chain molecule possessing functional groups at both ends or a functionalized polymer thin film.^{2,9,13,14} Monolayer-protected Au nanoparticles are known to self-assemble on solid surfaces leading to spontaneous formation of ordered 2D or 3D structures.^{14–16} Monolayer-protected Au nanoparticles in solution or on an electrode surface exhibit, for example, a stepwise charging process with a capacitance per particle of an order of attofarads, and the Au particles are expected to behave as quantum dots.^{6,10,16–18} Au particles deposited on an electrode surface also provide a nanostructured interface useful for spectroelectrochemistry. To mention just few examples, a thin layer composed of interconnected Au particles on a prism can be used as a substrate for the surface-enhanced IR absorption measurement in an internal reflection configuration.¹⁹ A Au thin film, on which Au particles of 30–60 nm diameters are deposited, has been examined as the substrate for surface plasmon resonance spectroscopy.²⁰

In the researches targeting the fabrication of the functional electrode surfaces using metal nanoparticles, it is important to

establish in situ methods to evaluate particle charge, position (e.g., distance from the substrate surface), and aggregation state, as well as microenvironment such as the interfacial static field felt by the particles. Clarification of potential distribution at an electrode/organic monolayer/metal nanoparticle layer/solution interface should also be of tremendous importance for the understanding of electrochemical properties of the interface, though investigation on this point has not been reported. The aim of this paper is to describe what we can see at such an interface using the potential-modulated UV–vis reflectance spectroscopy (electroreflectance spectroscopy). Gold nanoparticles show a plasmon absorption band in the visible wavelength region, and the absorption spectrum is sensitive to the particle size.^{21–24} Other factors such as particle charge, aggregation state, and physicochemical microenvironment of the surrounding medium may also modify the plasmon absorption characteristics.^{23–27} Not only the static interfacial structure of a Au particle layer but also the dynamic interfacial behavior of the particles is of our exceptional interest to be explored by the use of electroreflectance (ER) measurements.

Foss and his colleagues found the change of the plasmon absorption characteristics of Au particles deposited on a semiconductive SnO₂ optically transparent electrode with the change in electrode potential.^{3,4,8} The plasmon absorption band was red-shifted and became weaker when the electrode potential was moved to positive. This change depended on the particle size and electrolyte anion. Potential-dependent plasmon bands in the transmission absorption spectra at electrode surfaces were also reported for Ag⁵ and Au particles.^{7,11,12} Schiffrin and his colleagues are the first who reported ER spectra of Au particles in self-assembled multilayer thin films where the particles are linked with dithiol molecules.^{7,28} They observed an ER band

* To whom correspondence should be addressed. E-mail: sagara@net.nagasaki-u.ac.jp. Fax: (+81) 95-843-7271.

† PRESTO, JST.

‡ Nagasaki University.

around plasmon absorption wavelength, though they did not describe the characteristics of the ER signal in depth.

Electroreflectance spectroscopy can monitor small changes of the reflectance or absorbance in response to an ac potential modulation.²⁹ The sensitivity is high enough to monitor a 10⁻³% change of the reflectance. Additionally, the ER method can be used to track the dynamic behavior as long as the process originating the reflectance change is chemically reversible under the potential modulation. In the use of the ER method, it is unnecessary to adopt a transparent substrate. This provides us with an opportunity to characterize the plasmon absorption of metal particles immobilized on nontransparent metal electrodes.

We describe herein the result of ER characterization of a sub-monoparticle layer of 11 nm Au particles on an organic monolayer coated on a polycrystalline Au electrode. A multiple particle layer was avoided to simplify the interfacial structure. This particle size gives a plasmon absorption band strong enough to be sensitively measured as a reflectance signal. Citrate-stabilized particles were used to avoid a strong damping effect on the plasmon absorption as observed with alkanethiol-modified Au nanoparticles.³⁰ As a surface modifier forming the organic monolayer, aminoundecanethiol (1-mercapto-11-aminoundecane, abbreviated as "AUDT" in the present paper) was used.

Experimental Section

Chemicals. HAuCl₄·4H₂O (Hayashi Pure Chemicals) and trisodium citrate dihydrate (Kanto Chemicals) were reagent grade and used as received. AUDT supplied from Dojindo as a hydrochloric acid salt was used without further purification. Water was purified through a Milli-Q Plus Ultrapure water system (Millipore Co.). Its resistivity was over 18 MΩ cm. All other chemicals were of reagent grade and were used without further purification. The phosphate buffer solution was prepared from potassium salts.

Preparation of Au Particles. In 100 mL of water containing 1.17 mM HAuCl₄, 17 mL of 1% trisodium citrate dihydrate aqueous solution was added within a period of 5 s while refluxing with vigorous stirring under a nitrogen atmosphere. The immediately formed Au colloidal solution of wine red color was kept refluxing for a period of 1 h and then left to cool to room temperature. The resulting Au colloidal solution showed an absorption maximum at 518.5 nm (see Figure 3A). For UV-vis spectroscopic measurements, a spectrophotometer (Hitachi U-3000) was used. Statistical treatment of over 100 particles in the TEM image (Figure 1, inset) gave average and deviation of the particles' diameter as being 11.5 and 1.5 nm, respectively. Any agglomerated particle was not seen in the TEM image. For the TEM observation, an electron microscope (JFC-100, JEOL) was employed at an accelerated voltage of 100 kV.

Preparation of Organic Monolayer and Immobilization of Au Colloidal Particles. A polycrystalline Au disk electrode (geometrical area, 2.01 mm²; purchased from BAS Co.) was polished to a mirror finish by the subsequent use of 0.3 and 0.05 μm alumina suspensions. The polished Au electrode was immersed in an ethanolic solution of AUDT for a period of at least 90 min. The AUDT monolayer-modified Au electrode was rinsed well with ethanol and dipped in a Au colloidal solution (24 nM Au solution) under stirring. Finally, the resulting electrode was rinsed with a copious amount of water and subjected to the electrochemical and ER measurements.

Quartz Crystal Microbalance (QCM) Study. An AT-cut quartz plate with overlying Au coats at both sides (QA-A9M-Au, Seiko EG&G Co.) with a fundamental resonance frequency of 9 MHz was used as a QCM tip by combining a resonator/

frequency analyzer (QCA917-20, Seiko EG&G Co.), which was computer-controlled by WinEchem software (Seiko EG&G). One side of the Au film surface was exposed to the solution for the weight change measurements. The QCM tip, the surface of the Au film of which was modified with an AUDT monolayer, was first equilibrated in stirred pure water, and then Au colloidal solution was injected into the water under stirring. The final concentration of Au solution was 2.4 nM.

Atomic Force Microscope (AFM) Observation. The morphology of the Au particles deposited on an AUDT monolayer was visualized by the use of an AFM in air. The AUDT monolayer preparation on a vacuum-evaporated Au film on a quartz substrate (Auro Sheet (111)HS, Tanaka Novel Metals Co.) was followed by the immobilization of Au particles. The Au film surface was highly enriched with (111) terraces. A scanning microprobe system (SPI3800N, Seiko Instrumental Co.) was employed with a Si₃N₄ probe (canti lever SN-AF01, Seiko Instrumental Co.).

Electroreflectance Study. A quartz spectroelectrochemical cell was used for both voltammetric and ER measurements. The instrumentation used for ER measurements is described elsewhere.²⁹ A polarizer (Sigma Koki, extinction ratio 1/10 000 in the 300–700 nm region) was used when irradiating p- or s-polarized light. The waveform modulating the electrode potential E is described as

$$E = E_{dc} + E_{ac} = E_{dc} + \Delta E_{ac} \exp(j\omega t) \quad (1)$$

where E_{dc} is the dc potential, E_{ac} is the ac potential, ΔE_{ac} is the ac amplitude, $j = \sqrt{-1}$, $\omega = 2\pi f$, which is the angular frequency (f is the frequency of the potential modulation), and t is the time. The ER signal is defined as the ac component of the reflectance divided by the time-averaged reflectance and designated as $\Delta R/R$. Both the real part (in-phase component with respect to E_{ac}) and the imaginary part (90° out-of-phase component) of $\Delta R/R$ were monitored simultaneously as a function of either the incident light wavelength, λ , or f .

Electrochemical Measurements. As the reference and counter electrodes, a Ag/AgCl/saturated KCl solution and a Au wire coil were used, respectively. All of the potentials cited in this paper are referenced to this reference electrode. All measurements were made in an argon (>99.998%) atmosphere at 23 ± 2 °C. For the impedance and ER measurements, a lock-in amplifier (EG&G, model 5210) was employed for the phase-sensitive detection of the signals.

Results and Discussion

1. Deposition of Au Particles as Tracked by QCM and as Observed by AFM. Figure 1 shows a typical time course of the QCM response. When Au solution was injected in stirred water, the resonance frequency of the QCM tip modified with an AUDT monolayer started decreasing and finally tended to saturation. The frequency change, Δf , is proportional to the weight gain according to the Sauerbrey equation with a slope of -1.068 ng/Hz. Assuming that the rate of the deposition of Au particles is proportional to the remaining area on the Au substrate available for further deposition and that no displacement of Au particles takes place once deposited, the transient of the QCM response is expressed as

$$W(t) = W_s [1 - \exp(-kt)] \quad (2)$$

where $W(t)$ is the total weight of the Au particles deposited on the Au substrate at time t , k is the rate constant, and W_s is the saturated weight. The experimental $W(t)$ versus t curve in Figure

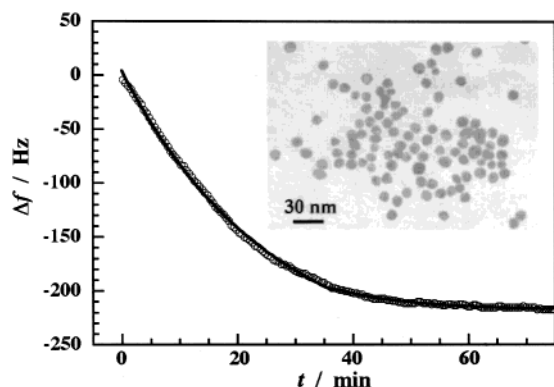


Figure 1. Plot of the QCM frequency shift, Δf , as a function of time, t , after the injection of Au solution in pure water at a preimmersed AUDT-modified Au layer-coated QCM tip. The water was kept stirred. The final concentration of the Au particles in water was 2.4 nM. Circles represent experimental data; the solid line represents the best fit curve for eq 2. The inset shows a TEM image of the Au particles on a collodion film.

1 fit well to eq 2, giving a linear correlation coefficient of $R^2 = 0.9992$ as the result of regression analysis. The best fit parameters were $W_s = 286$ ng and $k^{-1} = 25.5$ min. Good agreement of the experimental data with eq 2 indicates that the above assumptions actually hold. The presence of the saturated value of W means that the Au particles are attracted with the monolayer-covered surface while interparticle interaction between negatively charged particles is repulsive.

Although we could not calibrate the real surface area of the Au surface on the QCM tip, it is worthwhile to comment on the value of W_s . If the Au particles with an 11 nm diameter form a monolayer in a 2D hexagonal close-packing structure, the coverage should be 9.7×10^{11} particles cm^{-2} . The experimental value of W_s corresponds to 1.08×10^{11} particles cm^{-2} using a geometrical surface area of the substrate, regardless of the Au solution concentration. This fact indicates that the experimental saturated coverage is approximately 1/10 of the close-packing coverage. Smaller values than the close-packing coverage may be due to the interparticle repulsion,³¹ though we cannot exclude the possibility that a fraction of the terminal primary amine groups were reacted with atmospheric O_2 or CO_2 ,³² resulting in the partial loss of the ability to bind to Au particles. Natan and his colleagues reported that the deposition rate is controlled by the diffusion of the particles under a quiescent condition.³¹ Under the present stirring condition, the overall rate of deposition was strictly governed by the deposition step but not by the mass-transfer step.

Figure 2 represents typical AFM images obtained on an AUDT-modified Au(111) substrate. Further deposition of a Au particle overlaid on the underlying Au particles was seldom seen. Long-range aggregation of individual particles was not found. The apparent average diameter of the Au particle was seen to be greater than the diameter obtained from the TEM image. The cone shape of the AFM tip may result in a larger apparent diameter. The Au particle coverage in the AFM image is 10–12% with respect to the close-packing structure, in accordance with the QCM data. When zooming out, we did not see any two-dimensional pattern such as that observed on an amine-terminated silane film.³³

2. Electroreflectance Spectrum. Figure 3A shows the absorption spectrum of the Au colloidal solution. The peak wavelength of the plasmon absorption band at 518.5 nm corresponds well to the TEM diameter in light of the reported relationship between the peak wavelength and the particle diameter.^{2,22,34,35}

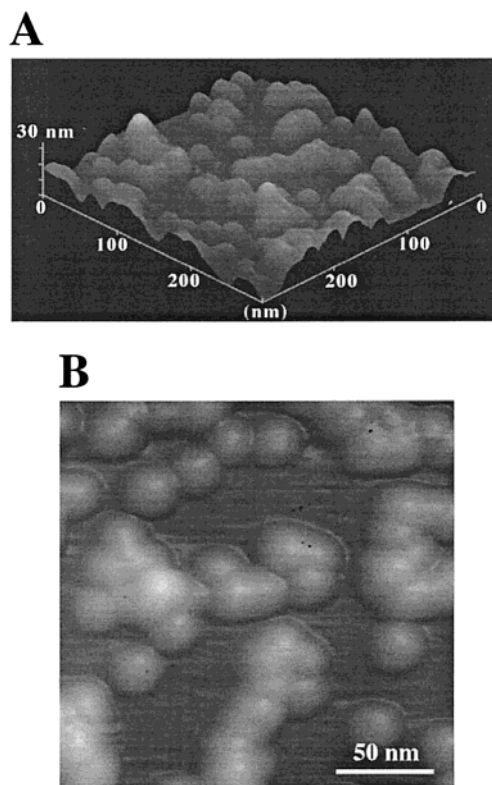


Figure 2. AFM images (A and B) of the Au particle-immobilized AUDT-modified Au(111) surface.

The line b in Figure 3B represents the ER spectrum of an AUDT-modified Au electrode before Au particle immobilization. This spectrum possesses a minimum at 545 nm. The signal is almost zero at the wavelengths shorter than 475 nm. These features are different from the spectrum of a bare Au electrode (line a), which shows a typical ER profile of a bare polycrystalline Au electrode.³⁶ The decrease of the intensity by modification with AUDT is a usual phenomenon for thiol adsorption on a Au electrode surface.³⁶

The ER spectrum of a Au particle-immobilized AUDT-modified Au electrode at $E_{dc} = 0.1$ V (Figure 3C) showed a positive-going ER band with a maximum at 528 nm, a 10 nm longer wavelength than the absorption maximum of the Au colloidal solution (Figure 3A). The ER band peak wavelength depended on E_{dc} (vide infra).

We examined the dependence of this ER signal on the polarization type of the incident light and the incident angle. As the results, the spectral profile was almost insensitive to both the polarization type (p- or s-polarized) and the incident angle in the range of 22–41° with respect to the surface normal. The observed p/s ratio of the ER signal always ranged between 1.2 and 1.4. If the ER signal was mainly due to the light reflection at the Au particle overlayer on the AUDT monolayer rather than the light absorption of the particles, we should have observed a much greater p/s ratio with much steeper dependence on the incident angle. For the former optical process, the spectrum is determined by the spectra of both real and imaginary parts of the refractive index of the overlayer within a continuum phase approximation, which is valid at much longer wavelengths than the particle size. We also measured the spectrum of the time-averaged intensity of the reflected light at a constant potential. No apparent difference of the spectral curve between the absence and presence of the Au particle overlayer was detected within the instrumental sensitivity. These results indicate that the ER spectrum represents the absorption spectrum

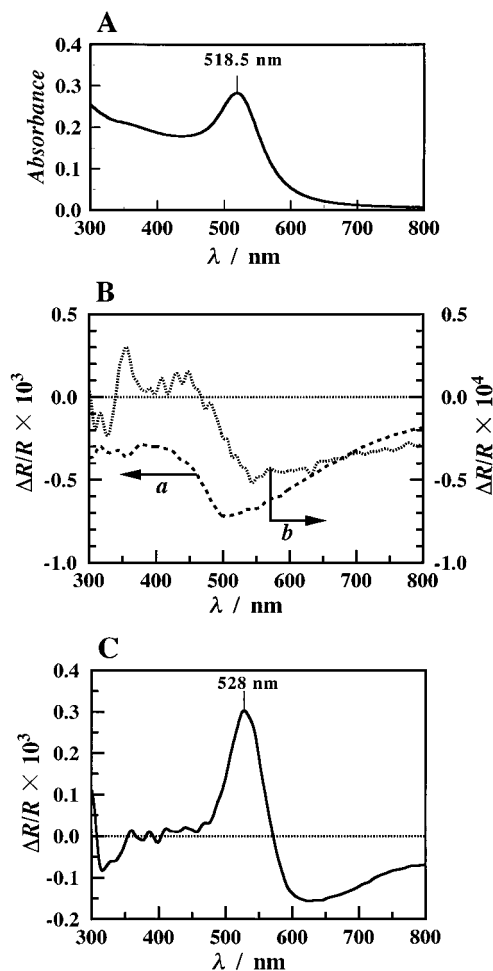


Figure 3. Absorption spectrum (A) of 24 nM Au solution with the light path length of 10.0 mm, ER spectra (B) (real part) of a bare Au electrode (line a) and of an AUDT-modified Au electrode (line b) (dipping time in AUDT ethanolic solution was 24 h) and ER spectrum (C) (real part) for a Au particle-immobilized AUDT-modified Au electrode (dipping time in AUDT ethanolic solution was 18 h and in Au solution 90 min). Conditions of ER measurements were $E_{dc} = 0.10$ V, $\Delta E_{ac} = 99$ mV, $f = 14.0$ Hz. Incident angle of the nonpolarized light was 32° . The electrolyte solution was 0.1 M phosphate buffer, pH 7.01.

of the Au particles at more negative potential from which that at more positive potential is subtracted within the range of the potential modulation

The positive-going plasmon absorption ER band indicates that the plasmon absorption is enhanced when the potential is shifted to more negative values. The ER spectrum also has a negative-going portion at the wavelengths longer than 580 nm. Compared to line b in Figure 3B, the longer wavelength ER signal is stronger. Therefore, this negative-going ER signal also arises from the Au particle.

The imaginary part of the obtained ER spectrum represented a factored mirror image of the real part with respect to the zero line, regardless of f in the range from 4 Hz to 2 kHz. The ER spectral structure did not depend on f . The imaginary part of the ER signal is the 90° out-of-phase component of the ac reflectance change with respect to the ac potential modulation. When the observed ER signal consists of, for example, two different components and one of them is due to a kinetically faster process than the other, the relative contribution of the slower process to the imaginary part of the ER signal is greater than that of the faster process. Then, the imaginary part differs from the real part in spectral structure, if these individual

processes give different spectral shapes. Therefore, these facts reveal that the ER signal obtained in the present work consists of a single component, or even if it consists of multiple components, their frequency dependencies (i.e., kinetics) should be identical.

Baum and his colleagues have reported an ER spectrum of a double-layered 1,10-decanedithiol/Au particle (6 nm)-modified Au electrode.⁷ In their spectrum, the ER band also appeared near the plasmon absorption wavelength, though the band is negative-going, in sharp contrast to our results. In ref 7, the ER signal for the bare Au electrode around 500 nm and that for the surface plasmon maximum are both negative-going, while the latter is positive-going in the present study. The origin of this difference is not sure at present but is possibly due to the difference in the definition of the sign of the ER signal. Foss and his colleagues measured the transmission absorption spectrum of Au particles physisorbed on a SnO₂ electrode in various electrolyte solutions and found that the plasmon absorption band becomes smaller with a red-shift with shifting the electrode potential to positive.⁴ The sign of our ER spectrum is in line with their observation.

3. Features of Electroreflectance Signal. The peak wavelength of the positive-going ER band, λ_p , is close to the plasmon absorption maximum of the Au colloidal solution of 518.5 nm in the range of E_{dc} from -0.5 to -0.1 V (Figure 4A). At less negative potentials, λ_p shifts to longer wavelength, up to 530 nm at 0.2 V. At further more positive potentials, λ_p became shorter than that at 0.2 V.

The plasmon absorption wavelength of Au particles is not necessarily identical with that of the absorption maximum of the Au colloidal solution. The wavelength depends on the aggregation state, interparticle interaction, dielectric constant of the medium, the particle charge, or some other factors.^{5,8,23–27,37,38} One or combinations of these factors can be the function of E_{dc} , giving rise to the observed λ_p - E_{dc} curve.

The potential dependence of the ER signal intensity is represented by the plot of ER peak height of the real part signal as a function of E_{dc} (Figure 4B). The intensity exhibited a maximum at 0.35 V.

Both parts A and B of Figure 4 show a peak near the potential of zero charge, E_{pzc} , of a bare polycrystalline Au electrode substrate. If the wavelength shift of the plasmon absorption band with the modulation of E was solely the origin of the ER signal, the ER intensity should have taken a maximum at the potential of the steepest λ_p - E_{dc} curve (around 0.0 V as seen in Figure 4A). Additionally, the ER spectral profile should have been of bipolar character at the plasmon band wavelength. However, both Figures 3C and 4B are not in line with these predictions. Thus, the ER signal is not due solely to the shift of plasmon band position with the potential, but plasmon absorption band intensity also depends on the potential.

The potential dependence is more explicitly seen by ER voltammograms (Figure 4C). There is little hysteresis in forward (cathodic) and backward scans, indicating that a potential-dependent attaching/detaching process of the Au particles is not the origin of the potential dependence of the ER signal intensity. In fact, as long as measurement potential range was restricted between -0.6 and 0.6 V, the ER signal was stable for hours. These facts also deny an adsorption-desorption process of citrate on the Au particles' surface as the origin of the ER signal. Otherwise, the ER signal should decrease steeply with time because a fraction of desorbed citrate should diffuse away to the bulk solution upon desorption.

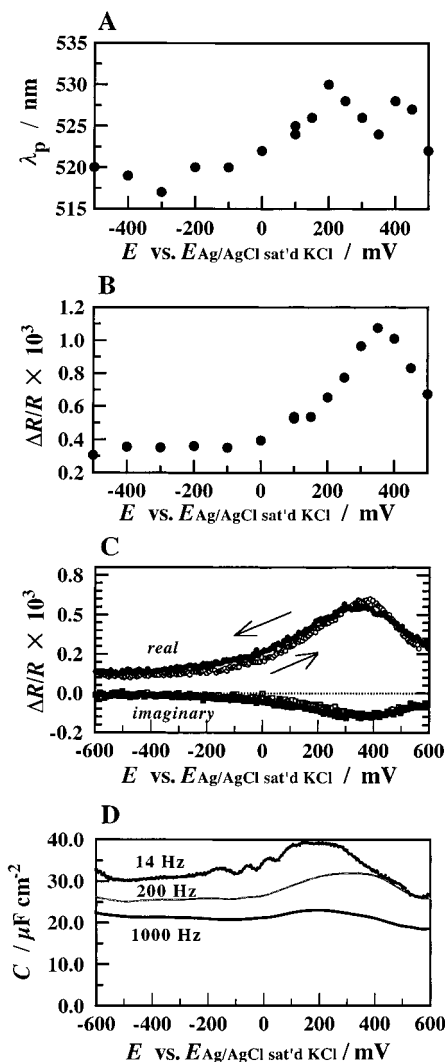


Figure 4. Potential dependence of the characteristics of the ER signal (A–C) and capacity–potential curve (D) for a Au particle-immobilized AUDT-modified electrode in 0.1 M phosphate buffer, pH 7.01. Panel A shows a plot of the peak wavelength of the ER band, λ_p , around the plasmon absorption as a function of E_{dc} . λ_p was obtained from ER spectra measured under the same conditions as Figure 3. Panel B shows a plot of the ER peak height of the real part at λ_p as a function of E_{dc} . Measurement conditions were the same as panel A. Panel C shows the cyclic ER voltammogram at $\lambda = 530$ nm, $\Delta E_{ac} = 99$ mV, $f = 14$ Hz, and a sweep rate of ± 2 mV s^{-1} . Panel D shows the differential capacity (C)–potential curves at three different frequencies. C was obtained from ac voltammograms at $\Delta E_{ac} = 7.1$ mV using a presumed equivalent circuit in which the capacity is connected in series with a resistance.

The interfacial differential capacitance, C – E_{dc} , curves (Figure 4D) exhibited a peak around 0.2 V, roughly corresponding to E_{pzc} . The rate of the change of the interfacial charge is greatest around this potential. The dc potential dependence of the ER signal intensity is in line with the potential dependence of the magnitude of the change of the interfacial charge.

These results in Figure 4 indicate that the dominant factor governing the ER signal exhibits the steepest potential dependence around E_{pzc} , keeping in mind that ER signal is the differential quantity with respect to E . The change of the electrode potential may alter not only the interfacial electric field but also the particle charge. The increase of the negative charge on a Au particle at more negative potentials results in the increase of the electron density in the particle. Then, the plasma frequency of the electrons increases. The change of the plasma frequency may also be accompanied by an increase in

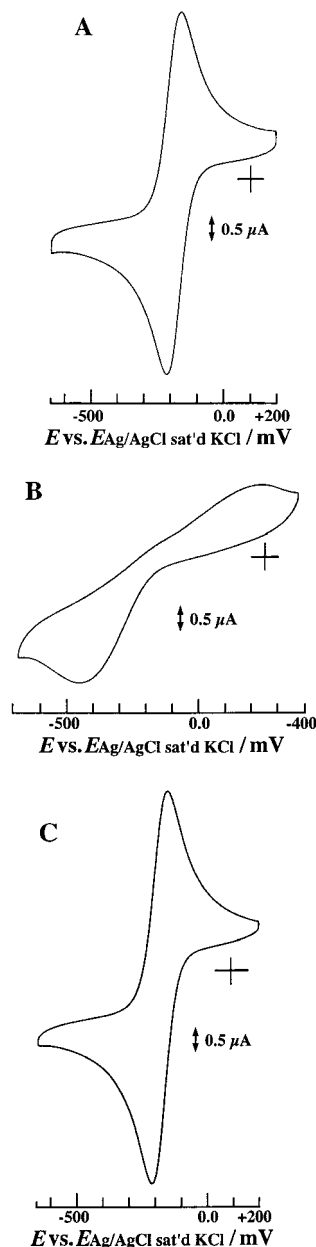


Figure 5. Cyclic voltammograms of 1 mM $[Ru(NH_3)_6]Cl_3$ at 0.1 V s^{-1} in 0.1 M phosphate buffer solution (pH 7.1): (A) bare Au electrode; (B) AUDT-modified Au electrode; (C) Au particle-immobilized AUDT-modified Au electrode.

the absorption coefficient of the Au particles through the change in the dielectric function of the Au particle. In fact, the sign of the ER signal (positive-going) is indicative of the increase of the absorption coefficient of the Au particle at more negative potentials. Taken together, it is likely that the charge on the Au particle is a function of the electrode potential as long as the particles attain good electronic communication with the electrode substrate.

4. Electrochemistry of Solution-Phase Species. To examine the electronic communication between immobilized Au particles and the electrode substrate, voltammograms of solution-phase species at a Au particle-immobilized AUDT-modified Au electrode were measured. At a bare Au electrode, hexaammine-ruthenium(II/III) ion ($[Ru(NH_3)_6]^{2+/3+}$) exhibited an electrochemically-reversible voltammogram at a sweep rate, ν , of 0.1 V s^{-1} (Figure 5A). The apparent diffusion constant, D_{app} , calculated by the use of the geometrical electrode surface area

was $4.6 \times 10^{-6} \text{ cm}^2 \text{ s}^{-1}$. An AUDT-modified Au electrode showed a cyclic voltammogram (CV) with a peak separation, ΔE_p , greater than 650 mV at $\nu = 0.1 \text{ V s}^{-1}$ (Figure 5B), indicating that the electrode reaction is highly irreversible. This is due to the sluggish electron-transfer kinetics through the AUDT monolayer. The terminal amino groups are partially protonated and charged positively, contributing to the electrostatic repulsion between the monolayer surface and hexammineruthenium cations in the solution phase. When Au particles were deposited on the AUDT monolayer, the CV appeared electrochemically reversible (Figure 5C) with $\Delta E_p = 60 \text{ mV}$ and $D_{\text{app}} = 5.4 \times 10^{-6} \text{ cm}^2 \text{ s}^{-1}$, almost the same as that obtained for a bare electrode. This fact reveals that the Au particles on the AUDT monolayer act collectively as the new electrode surface and that the particles achieve good electronic communication with the underlying Au substrate. The almost reversible CVs were also obtained in 1 mM $\text{K}_3[\text{Fe}(\text{CN})_6] + 0.2 \text{ M Na}_2\text{SO}_4$ ($\Delta E_p = 80 \text{ mV}$ at $\nu = 0.1 \text{ V s}^{-1}$) and in 1 mM methyl viologen + 0.1 M phosphate buffer solution ($\Delta E_p = 60 \text{ mV}$ at $\nu = 0.1 \text{ V s}^{-1}$). The reversible redox reaction was also reported by Schiffrin and his colleagues for a Au particle bilayer on a Au electrode.⁷ The total projection area of Au particles when the coverage is 10% of the 2D close-packing structure is 9% of the substrate area. The CV should become a sigmoidal wave because of the radial diffusion at ν greater than 10^5 V s^{-1} , provided that interparticle distance is homogeneous. Therefore, it is reasonable that we obtain a diffusion-controlled CV wave at $\nu = 0.1 \text{ V s}^{-1}$ as though the electrode is planar.

5. Frequency Dependence of Impedance and ER Signal.

The results of the previous sections indicate that the optical properties of the immobilized Au particles depend on the electrode potential. One can track the dynamics of the changes of the optical properties by the ER method in the frequency domain. For example, if the ER signal is due to the change of the interfacial electric field felt by the Au particles, the ER signal should follow the change of the interfacial electric field without any delay. The ER signal represents the field-modulated change of the optical constant in such a case. The frequency dependence of the ER signal was measured and compared with the impedance data. (The frequency dependence may also be potential-dependent as seen in Figure 4C; the ratio of real and imaginary part ER signals depends on E_{dc} . We do not go into details of the potential dependence of the dynamics in the present paper.)

Figure 6A shows a complex plane plot of the impedance for a Au particle-immobilized AUDT-modified electrode. The plot is typical of a double-layer feature. Complex plane plot of the ER signal (Figure 6B) exhibited a part of a semicircle in the high-frequency region, but the trajectory exhibited a significant tailing to the real part axis at low frequencies. With the use of an uncompensated resistance, $R_s = 265 \Omega$, obtained by extrapolating the impedance plot of the high-frequency limit to the real axis, the ER signal as a function of f was analyzed as follows. We assumed a simple equivalent circuit in which the interfacial impedance Z_1 is in series with R_s (see inset of Figure 6A). Through the use of the measured impedance, the ac voltage across Z_1 , which is designated as e_1 , is obtained as being

$$e_1 = E_{\text{ac}}(1 - R_s/Z) \quad (3)$$

where Z is the total impedance.

Figure 7 compares the frequency dependence of e_1 to that of the ER signal. The frequency at the minimum of the imaginary part of e_1 corresponds to the reciprocal of the cell time constant divided by 2π . Three characteristic frequencies of the ER signal,

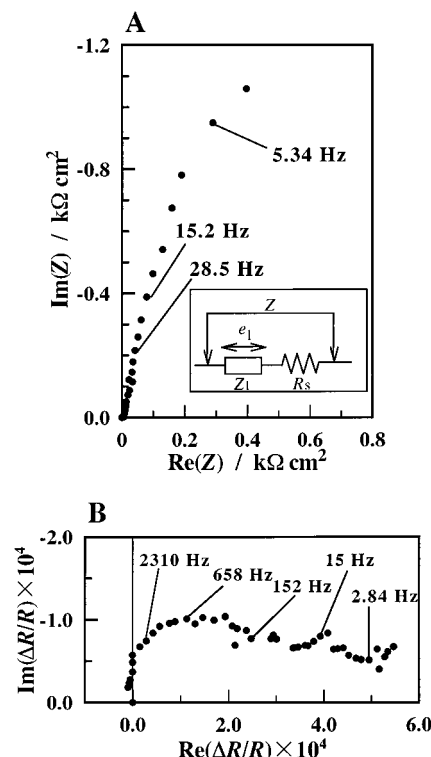


Figure 6. Complex plane representations of the frequency dependence of ac impedance and ER signal: (A) complex plane plot of ac impedance for a Au particle-immobilized AUDT-modified electrode in 0.1 M phosphate buffer, pH 7.01, with $E_{\text{dc}} = 0.30 \text{ V}$ and $\Delta E_{\text{ac}} = 7.1 \text{ mV}$. An equivalent circuit is shown in the inset. Panel B shows the complex plane plot of the ER signal for the same system with $E_{\text{dc}} = 0.30 \text{ V}$, $\Delta E_{\text{ac}} = 99 \text{ mV}$, and $\lambda = 528 \text{ nm}$.

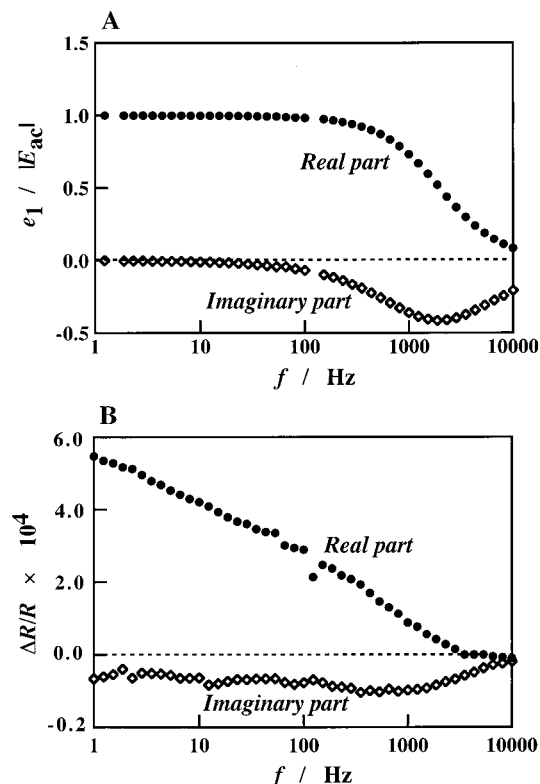


Figure 7. Bode plots of $e_1/|E_{\text{ac}}|$ (A) and the ER signal (B).

onset frequency, the frequency at the minimum of the imaginary part, and the frequency of the steepest real part-frequency curve, are all at smaller frequencies than those of e_1 . These facts

indicate that the ER signal does not directly synchronize with the modulation of the interfacial electric field. At the frequencies lower than 100 Hz, the interfacial electric field is frequency-independent and has no phase difference with E_{ac} . In contrast, the ER signal was still getting greater with decreasing the frequency. This fact indicates that the ER signal involves the contribution from a slow process (vide infra).

6. Implications of the ER Signal. We interpreted that the ER signal is due to a potential-dependent charging–discharging process of the immobilized Au particles in response to both potential modulation and dc potential, as described in Section 3. As far as the ER spectrum in the whole wavelength region is regarded as a difference absorption spectrum (absorption spectrum at more negative potential from which that at less negative potential is subtracted), the plasmon band was blue-shifted, the absorption intensity was increased, and the band was sharpened as the potential was made more negative. This interpretation can be consistently supported by the present experimental results as follows.

(1) The ER signal at the plasmon absorption wavelength is positive-going, indicating that the strength of the absorption increases as E_{dc} becomes more negative. When the electron density in a Au particle increases, the plasma frequency increases. As a result, the plasmon absorption is enhanced.

(2) Good electronic communication between the Au electrode substrate and the Au particles is attained. Because a polycrystalline Au substrate was used, it is plausible that a few particles are in direct contact with the Au underlayer at the monolayer defects providing electron-transfer pathways. However, if only these minor particles in contact with the substrate were responsible for the redox reactions of solution-phase species, the CV curves should appear sigmoidal as in the case of a microelectrode array even at a slow sweep rate because all of the particles are not interconnected as seen in the AFM image. If the numbers of monolayer defects or the Au electrode surface area directly exposed to the solution or both are considerable, the CV curve of an AUDT monolayer-modified electrode without Au particles should not be like Figure 5B. We also examined ER measurements using a Au electrode uncovered with an AUDT monolayer but preimmersed in a Au solution. As the result, no difference of ER spectrum was observed between before and after the immersion in the Au solution. The citrate-stabilized Au particle does not attach to a bare Au electrode surface, or even if it does, the particle does not produce an additional ER signal.

(3) For a metal electrode in a double-layer potential region, the change of the electrode surface charge per potential shift becomes greater as the potential is nearer to E_{pzc} . This potential dependence is also the case for an AUDT monolayer-modified electrode as shown by Figure 4D. Correspondingly, the ER signal becomes greater as E_{dc} becomes nearer to E_{pzc} . However, it is also possible that E_{pzc} for the Au particle is near to the substrate E_{pzc} .⁵

(4) The static electric field at the location of the Au particles is not the main origin of the ER signal as confirmed by Figure 7; the ER signal does not directly synchronize with the electric field. This supports also the absence of Au substrate–Au particle direct contact.

It has been reported that the plasmon absorption spectrum of a gelatin-adsorbed Au particle depends on the thickness or refractive index of the adsorbed polymer corona of the particle.³⁹ The spectral change in the report is not in line with our observation, indicating that these corona effects have little contribution to the ER spectral structure in the present system.

Yamada and her colleagues observed the change of the plasmon absorption band of an anthraquinone-derivative-attached 2.2 nm Au cluster deposited on an electrode surface: a blue shift of the plasmon absorption wavelength together with increased intensity as the shift of electrode potential in the negative direction.¹² Their results were interpreted in the context of negative charge (electron) accumulation on the Au core at more negative potentials, as theoretically and experimentally supported by Templeton and his colleagues.¹¹ The trends of the potential dependence are identical with our observation by ER methods. The potential-dependent plasmon absorption spectrum due to a charging–discharging process was previously reported for Ag particles in an optically transparent thin-layer electrochemical (OTTLE) cell by Ung and his colleagues, in line with our ER results.⁵ Ali and Foss also reported the plasmon spectral red shifting and intensity damping for Au nanoparticles adsorbed on transparent electrodes. Although their interpretation is, in principle, not as the charging–discharging process, the phenomenon they observed is identical with our observation by the ER method with regard to the potential dependence.⁴

Two effects of the charge transfer on the plasmon polariton excitation as the results of interaction of metal nanoparticles with its surroundings have been known: the static and dynamic charge transfer. The present study showed that more negatively charged Au particles exhibit a stronger and sharper plasmon absorption band at a shorter wavelength. The bandwidth is affected by the dynamic charge transfer.^{23,24,27} In the present case, the decrease in the number of conduction electrons in the particle may induce the band broadening through the dynamic charge-transfer effect. As for the static charge-transfer effect, the shift of λ_p per 1 V change of the electrode potential is approximately 12 nm (Figure 4A). On the basis of the proposed theory of the effect of the static charge transfer on the plasmon band position,^{23,27} the transferred charge should amount to roughly 10^3 electrons for an 11 nm Au particle. Assuming that the capacity of the particle can be estimated by the use of the double-layer differential capacity of the Au particle ($30 \mu\text{F cm}^{-2}$ as for the case of a bulk Au electrode), approximately 800 electrons should be transferred to maintain the equipotential with the electrode substrate, provided that the particles are spherical. This quantitative but rough estimate may support our interpretation of the ER signal to a charging–discharging process.

It is known that interparticle interaction of Au nanoparticles in an electromagnetic field alters the plasmon absorption greatly. Schmitt and his colleagues reported experimental and theoretical spectra.³⁷ The reported change of the absorption spectrum is far greater than that observed in the present work. However, Figure 2 shows the presence of small aggregates. It remains undeniably that the change of the topology of aggregates with the potential modulation produces a part of the absorption spectral shift, resulting in the presence of a slow process (Figure 6B) on one hand. On the other hand, this slow process can also be due to the presence of some “cool” particles exchanging electrons very slowly with the electrode surface. For majority of the particles, the electron transfer is rapid so as to give a reversible redox reaction for solution-phase species (Figure 5C). Taken together, to gain deeper insight into the optical properties of Au particles at an electrochemical interface, one should clarify the extent of homogeneity and the movements of the particles.

Conclusion

Electroreflectance signals of Au nanoparticles, which were first reported by Schiffrin and his colleagues^{7,28} at an electrochemical interface, were studied in greater detail in the present

work at an aminoundecanethiol monolayer-modified Au electrode. The ER signal was interpreted as being mainly due to the charging–discharging process of the Au particles in response to the change of electrode potential. New findings in the present study include the positive sign of the ER signal, the stronger and sharper plasmon absorption band at more negative potentials in addition to its blue shift, and the way that the ER signal follows the ac potential modulation in the frequency domain. For the ER spectral structure to be fully addressed, the reflection spectrum at the electrode/organic monolayer/metal particle/solution interface should be deduced theoretically, though it is quite difficult at present because of the complexity of the interfacial structure. Nevertheless, the present work demonstrates that the ER method is useful for in situ analyses of the potential-dependent change and its dynamics of the metal particles at electrified interfaces and for sensing the physical and chemical nanoparticle interfacial properties⁴⁰ by the use of the plasmon absorption band (Mie resonance) as a probe. The charging–discharging process should be strongly influenced by the interfacial structure, and thus, the ER signal provides one of the keys to elucidate the structure. The advantageous features of the ER measurements of the plasmon absorption properties can be listed as follows: (i) a nontransparent electrode substrate can be used, (ii) the measurement is sensitive, even more sensitive than those reported by using transmission absorption spectroscopy,¹¹ (iii) information of dynamics can be obtained, and (iv) the ER method is applicable to the immobilized sub-monoparticle layer, appearing as a strong tool for the direct measurement of the electron transfer between the electrode surface and the particles dynamically.

Acknowledgment. In its initial stage, this work was in part financially supported by The Asahi Glass Foundation (to T.S.) and the Grant-in-Aid from the Ministry of Education, Science, Sports and Culture of Japan (to T.S.). The authors are grateful to Mr. S. Wakabayashi (NU) for his technical assistance.

References and Notes

- (1) (a) Brown, K. R.; Fox, A. P.; Natan, M. J. *J. Am. Chem. Soc.* **1996**, *118*, 1154. (b) Rubin, S.; Bar, G.; Taylor, T. N.; Cutts, R. W.; Zawodzinski, T. A., Jr. *J. Vac. Sci. Technol., A* **1996**, *14*, 1870. (c) Sun, Y. H.; Li, J. R.; Li, B. F.; Jiang, L. *Langmuir* **1997**, *13*, 5799. (d) Blonder, R.; Sheeney, L.; Willner, I. *Chem. Commun.* **1998**, 1393. (e) Horikoshi, T.; Itoh, M.; Kurihara, M.; Kubo, K.; Nishihara, H. *J. Electroanal. Chem.* **1999**, *473*, 113. (f) Gittins, D. I.; Bethell, D.; Nichols, R. J.; Schiffrin, D. J. *Adv. Mater.* **1999**, *11*, 737. (g) Musick, M. D.; Peòà, D. J.; Botsko, S. L.; McEvoy, T. M.; Richardson, J. N.; Natan, M. J. *Langmuir* **1999**, *15*, 844. (h) Shipway, A. N.; Lahav, M.; Blonder, R.; Willner, I. *Chem. Mater.* **1999**, *11*, 13. (i) Shipway, A. N.; Lahav, M.; Willner, I. *Adv. Mater.* **2000**, *12*, 993. (j) Kanayama, N.; Kitano, H. *Langmuir* **2000**, *16*, 577. (k) Bharathi, S.; Nogami, M.; Ikeda, S. *Langmuir* **2001**, *17*, 2001.
- (2) Doron, A.; Katz, E.; Willner, I. *Langmuir* **1995**, *11*, 1313.
- (3) Ali, A. H.; Luther, R. J.; Foss, C. A., Jr. *Nanostruct. Mater.* **1997**, *9*, 559.
- (4) Ali, A. H.; Foss, C. A., Jr. *J. Electrochem. Soc.* **1999**, *146*, 628.
- (5) Ung, T.; Giersig, M.; Dunstan, D.; Mulvaney, P. *Langmuir* **1997**, *13*, 1773.
- (6) Chen, S.; Murray, R. W. *J. Phys. Chem. B* **1999**, *103*, 9996.
- (7) Baum, T.; Bethell, D.; Brust, M.; Schiffrin, D. J. *Langmuir* **1999**, *15*, 866.
- (8) Gluodenis, M.; Manley, C.; Foss, C. A., Jr. *Anal. Chem.* **1999**, *71*, 4554.
- (9) Shipway, A. N.; Katz, E.; Willner, I. *CHEMPHYSICHEM.* **2000**, 18 and references therein.
- (10) Chen, S. *J. Phys. Chem. B* **2000**, *104*, 663.
- (11) Templeton, A. C.; Pietron, J. J.; Murray, R. W.; Mulvaney, P. J. *Phys. Chem. B* **2000**, *104*, 564.
- (12) Yamada, M.; Tadera, T.; Kubo, K.; Nishihara, H. *Langmuir* **2001**, *17*, 2363.
- (13) Grabar, K. C.; Allison, K. J.; Baker, B. E.; Bright, R. M.; Brown, K. R.; Griffith Freeman, R.; Fox, A. P.; Keating, C. D.; Musick, M. D.; Natan, M. J. *Langmuir* **1996**, *12*, 2353.
- (14) Schmid, G.; Bäuml, M.; Beyer, N. *Angew. Chem., Int. Ed.* **2000**, *39*, 181.
- (15) (a) Sato, T.; Brown, D.; Johnson, B. F. *Chem. Commun.* **1997**, 1007. (b) Hostetler, M. J.; Wingate, J. E.; Zhong, C.-J.; Harris, J. E.; Vachet, R. W.; Clark, M. R.; Londono, J. D.; Green, S. J.; Stokes, J. J.; Wignall, G. D.; Glish, G. L.; Porter, M. D.; Evans, N. D.; Murray, R. W. *Langmuir* **1998**, *14*, 17. (c) Brust, M.; Bethell, D.; Kiely, C. J.; Schiffrin, D. J. *Langmuir* **1998**, *14*, 5425. (d) Porter, L. A., Jr.; Ji, D.; Westcott, S. L.; Graupe, M.; Czernuszewicz, R. S.; Halas, N. J.; Randall Lee, T. *Langmuir* **1998**, *14*, 7378. (e) Whetten, R. T.; Shafiqullin, M. N.; Khoury, J. T.; Schaaff, T. G.; Vezmar, I.; Alvarez, M. M.; Wilkinson, A. *Acc. Chem. Res.* **1999**, *32*, 397. (f) Taleb, A.; Russier, V.; Courty, A.; Pileni, M. P. *Phys. Rev. B* **1999**, *59*, 13350. (g) Wang, Z. L. *J. Phys. Chem. B* **2000**, *104*, 1153. (h) Martin, J. E.; Wilcoxon, J. P.; Odinek, J.; Provencio, P. *J. Phys. Chem. B* **2000**, *104*, 9475. (i) Green, M.; O'Brien, P. *Chem. Commun.* **2000**, 183. (j) Teranishi, T.; Haga, M.; Shiozawa, Y.; Miyake, M. *J. Am. Chem. Soc.* **2001**, *122*, 4237. (k) He, S.; Yao, J.; Jiang, P.; Shi, D.; Zhang, H.; Xie, S.; Pang, S.; Gao, H. *Langmuir* **2001**, *17*, 1571. (l) Yonezawa, T.; Onoue, S.; Kimizuka, N. *Langmuir* **2001**, *17*, 2291.
- (16) Templeton, A. C.; Peter Wuelfing, W.; Murray, R. W. *Acc. Chem. Res.* **2000**, *33*, 27.
- (17) Chen, S.; Murray, R. W. *Langmuir* **1999**, *15*, 682.
- (18) Chen, S.; Templeton, A. C.; Murray, R. W. *Langmuir* **2000**, *16*, 3543.
- (19) Osawa, M. *Bull. Chem. Soc. Jpn.* **1997**, *70*, 2861.
- (20) Andrew Lyon, L.; Peòà, D. J.; Natan, M. J. *J. Phys. Chem. B* **1999**, *103*, 5826.
- (21) Kreibitz, U.; Fragstein, C. V. *Z. Phys.* **1996**, *224*, 307.
- (22) Link, S.; El-Sayed, M. A. *J. Phys. Chem. B* **1999**, *103*, 4212.
- (23) Kreibitz, U.; Bour, G.; Hilger, A.; Gartz, M. *Phys. Status Solidi A* **1999**, *175*, 351.
- (24) Kreibitz, U.; Vollmer, M. *Optical Properties of Metal Cluster*; Springer Series in Materials Science 25; Springer-Verlag: Berlin, 1995.
- (25) Shipway, A. N.; Lahav, M.; Rachel, G.; Willner, I. *Langmuir* **2000**, *16*, 8789.
- (26) Murakoshi, K.; Nakato, Y. *Jpn. J. Appl. Phys.* **2000**, *39*, 4633.
- (27) Hövel, S.; Fritz, S.; Hilger, A.; Kreibitz, U.; Vollmer, M. *Phys. Rev. B* **1993**, *48*, 18178.
- (28) Bethell, D.; Brust, M.; Schiffrin, D. J.; Kiely, C. J. *Electroanal. Chem.* **1996**, *409*, 137.
- (29) Sagara, T. *Res. Devel. Phys. Chem.* **1998**, *2*, 159.
- (30) Linnert, T.; Mulvaney, P.; Henglein, A. *J. Phys. Chem.* **1991**, *95*, 7843.
- (31) Grabar, K. C.; Smith, P. C.; Musick, M. D.; Davis, J. A.; Walter, D. G.; Jackson, M. A.; Guthrie, A. P.; Natan, M. J. *J. Am. Chem. Soc.* **1996**, *118*, 1148.
- (32) Spirk, M.; Delamar, E.; Michel, B.; Röthlisberger, U.; Klein, M. L.; Wolf, H.; Ringsdorf, H. *Langmuir* **1994**, *10*, 4116.
- (33) Haidara, H.; Mougín, K.; Schultz, J. *Langmuir* **2001**, *17*, 659.
- (34) Turkevich, J.; Garton, G.; Stevenson, P. C. *J. Colloid Sci.* **1954**, Suppl. 1, 26.
- (35) Brown, K. R.; Natan, M. J. *Langmuir* **1998**, *14*, 726.
- (36) Sagara, T.; Kawamura, H.; Nakashima, N. *Langmuir* **1996**, *12*, 4253.
- (37) Schmitt, J.; Mächtle, P.; Eck, D.; Möhwald, H.; Helm, C. A. *Langmuir* **1999**, *15*, 3256.
- (38) Connolly, S.; Rao, S. N.; Fitzmaurice, D. *J. Phys. Chem. B* **2000**, *104*, 4765.
- (39) Eck, D.; Helm, C. A.; Wagner, N. J.; Vaynberg, K. A. *Langmuir* **2001**, *17*, 957.
- (40) Kreibitz, U.; Gartz, M.; Hilger, A. *Ber. Bunsen-Ges. Phys. Chem.* **1997**, *101*, 1593.